Hydrodeoxygenation of Isoeugenol over Ni- and Co-Supported Catalysts

Christoffer Lindfors,[†] Päivi Mäki-Arvela,[†] Petriina Paturi,[‡] Atte Aho,[†] Kari Eränen,[†] Jarl Hemming,[†] Markus Peurla,[§] David Kubička,[∥] Irina L. Simakova,[⊥] and Dmitry Yu. Murzin*,[†]

[†]Johan Gadolin Process Chemistry Centre, Åbo Akademi University, Biskopsgatan 8, 20500 Turku, Finland
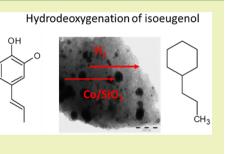
[‡]Wihuri Physical Laboratory, Department of Physics and Astronomy, University of Turku, Vesilinnantie 5, 20500 Turku, Finland

[§]Laboratory of Electron Microscopy, University of Turku, Kiinamyllynkatu 10, 20520, Turku, Finland

[∥]Department of Petroleum Technology and Alternative Fuels, University of Chemistry and Technology Prague, Technická 5, 166 28 Prague, Czech Republic

[⊥]Boreskov Institute of Catalysis, Lavrentieva 5, 630090 Novosibirsk, Russia

S *Supporting Information*

ABSTRACT: Hydrodeoxygenation (HDO) of isoeugenol was investigated over several Ni (Ni/SiO$_2$, Ni/graphite) and Co (Co/SBA-15, Co/SiO$_2$, Co/TiO$_2$, Co/Al$_2$O$_3$) catalysts at 200 and 300 °C under 30 bar hydrogen pressure in a batch reactor. The catalysts were prepared by an impregnation method and systematically characterized by X-ray diffraction, transmission electron microscopy, scanning electron microscopy and energy dispersive analysis, organic elemental, and thermogravimetrical analysis before and after the reaction. Analysis of the liquid, solid, and gaseous products was performed to identify isoeugenol transformation pathways. The maximum yield of the desired propylcyclohexane (PCH) (63%) and the highest sum of masses of reactants and products in the liquid phase based on GC results (GCLPA) (79%) were obtained over 10 wt % Co/SBA-15. HDO of isoeugenol over 11 wt % Co/SiO$_2$ resulted in 50% PCH yield with a rather similar GCLPA of 73%. Low yields of PCH and the liquid phase mass balance closure were obtained over highly dispersed 15 wt % Co/Al$_2$O$_3$ and 15 wt % Co/TiO$_2$. PCH yield was 60% over Ni/graphite and 44% over Ni/SiO$_2$ after 4 h with GCLPA values of 73 and 70%, correspondingly. Overall PCH yields increased in the following order: Co/TiO$_2$ < Co/Al$_2$O$_3$ < Ni/SiO$_2$ < Co/SiO$_2$ < Ni/graphite < Co/SBA-15. Regeneration and reuse of industrially relevant 11 wt % Co/SiO$_2$ was successfully demonstrated.

KEYWORDS: Hydrodeoxygenation, Isoeugenol, Cobalt catalysts, SBA-15, Propylcyclohexane, Regeneration
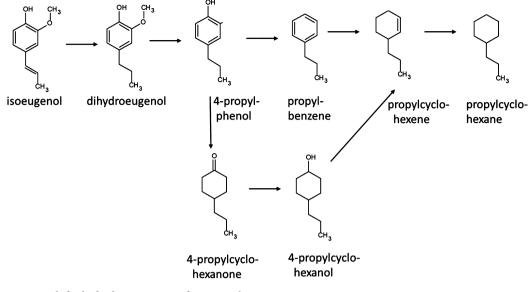
INTRODUCTION

Renewable resources supplied by solar power, geothermal energy, hydropower, wind power, and especially biomass are expected to increase in the near future, due to the desired reduction of fossil fuels consumption.[1] Of the above-mentioned renewable resources, biomass is still the only option for the liquid fuel production and can also be used for chemicals and energy production.[2] The importance of biofuels has not gone unnoticed, with the United States and the European Union both setting targets of 20% of transportation fuels to be obtained from biomass by 2030 and 2020, respectively.[3,4]
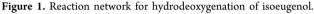
Biomass refers to materials produced in the natural life cycle. The most common of these materials are agricultural crops, wood, industrial waste, municipal waste, and food waste. Biomass has a potential to be used as a renewable resource compared to fossil fuels, due to the differences in the time scale of recovering carbon. Carbon originating from the natural life cycle has a maximum ten year recycling period, whereas fossil carbon has a recycling period of thousands of years. Because of

these differences in timespans, biomass utilization does not affect the carbon cycle.[5,6]

The main building blocks of biomass can be divided into four groups, mainly due to their molecular structures. These groups are carbohydrates (cellulose, hemicellulose, and starch), lignin, lipids, and proteins.[7,8] Together, cellulose, hemicellulose, and lignin form lignocellulosic biomass. Of these three, lignin has received the least attention in research for production of biofuels even though it is regarded as the aromatic resource of the biobased economy.[3]

Lignin in wood is one of the possible sources of aromatic monomers, which can be applied as a feedstock for production of cyclic hydrocarbons. Bio-oil produced by lignin pyrolysis is not suitable as a fuel due to its low stability in the presence of water and acids. Hydrodeoxygenation (HDO) of bio-oil has been already investigated;[9] however, it is very demanding due to a complicated analysis producing both water and organic

Figure 1. Reaction network for hydrodeoxygenation of isoeugenol.

phase products, humins, gaseous products, and char. In order to understand the reaction mechanism in HDO of phenolic compounds, several model compounds, such as guaiacol, anisole, and phenol has been intensively investigated.[10−12] Isoeugenol HDO has been studied over noble metal catalysts, containing Pt, Ir, and Ru.[13−16] The reaction network in hydrodeoxygenation of isoeugenol is rather complex giving a range of products (Figure 1). Over noble metal catalysts the HDO of isoeugenol proceeds rapidly forming as a main product a fully deoxygenated product, propylcyclohexane already at 200 °C under 30 bar hydrogen.[13] Recently Pd, Rh, Pt, and Ru catalyzed HDO of lignin monomers has been demonstrated.[15,16]

Supported Ni- and Co-catalysts were investigated in this work in HDO of isoeugenol. These transition metals are cheaper in comparison to noble metals and have been used in HDO of several phenolic compounds.[12,17−21] In guaiacol HDO nickel nanoparticles were used and the main product was phenol at 350 °C under 5 bar hydrogen in a continuous reactor.[20] Furthermore, guaiacol HDO gave as the main product phenol over Ni−Al₂O₃−SiO₂ catalyst at 300 °C under 50 bar hydrogen[19] showing a difficulty to completely deoxygenate guaiacol, which was also indicated in ref 2. Ni-sulfated zirconia was used as a catalyst for a mixture of cresol, phenol, eugenol, trans-anethole, and vanillin.[21] The results revealed that eugenol was completely converted in this mixture mainly to propylcyclohexane under 50 bar hydrogen at 300 °C in 8 h.[21] Ni/SiO₂ catalyst facilitated in phenol HDO production of cyclohexane with 86% selectivity at complete conversion of phenol under 50 bar hydrogen at 300 °C.[12] In addition Ni/ZrO₂ was also recently investigated in isoeugenol HDO at 250 °C under 30 bar hydrogen showing, however, that this catalyst is not suitable for isoeugenol HDO, since a low liquid phase mass balance closure was obtained.[17] In our recent work[18] high yield of propylcyclohexane, 75%, in isoeugenol HDO at 300 °C under 30 bar total pressure was obtained over Ni supported on mesoporous SBA-15.

On the other hand, Co/TiO₂ was inefficient to deoxygenate eugenol at 200 °C under 12 bar hydrogen in dodecane as a solvent[22] at complete conversion and the main product was propylcyclohexanol. Most probably the reaction temperature was too low for HDO over Co supported catalyst.

In this work Ni/SiO₂ and Ni/graphite were investigated in isoeugenol HDO and compared with the performance of Ni/SBA-15.[18] In addition, according to our knowledge, HDO of isoeugenol is performed for the first time in the current work over Co/SiO₂, Co-SBA-15, Co/Al₂O₃, and Co/TiO₂. A special emphasis was put on the estimation of catalyst resistance to coking through characterization of spent catalysts by thermogravimetric analysis, and organic elemental analysis as well as extracting coke with heptane and analyzing organic extracted components by size exclusion chromatography to reveal the presence of oligomers. In addition catalyst regeneration and reuse was successfully demonstrated.

■ EXPERIMENTAL SECTION

Catalyst Synthesis. Six different catalysts, both nickel and cobalt supported on SBA-15, SiO₂, TiO₂, Al₂O₃, and graphite were investigated in hydrodeoxygenation of isoeugenol. SBA-15, TiO₂, and Al₂O₃ supported Co catalysts were synthesized applying hexahydrate of cobalt nitrate as a precursor. The required amount of Co(NO₃)₂·6H₂O was dissolved in 100 mL of distilled water and added to a round flask containing the support. The resulting mixture was then stirred for 60 min at 25 °C using a horizontal shaker, after which the surplus water was evaporated under vacuum using a rotator−evaporator. The wet support containing cobalt nitrate was then dried at 100 °C for 2 h. To prepare silica supported catalysts SiO₂ was calcined at 550 °C for 3 h and impregnated with aqueous solutions of Ni(NO₃)₂·6H₂O or Co(NO₃)₂·6H₂O, correspondingly. The impregnated samples were then dried at 106−107 °C for 12 h and calcined in air at 550 °C for 3 h. Decomposition of nickel and cobalt nitrates was monitored by measuring the pH value of outcoming gases by a litmus indicator.

Catalytic Experiments and Analysis. The HDO experiments were carried out in a 300 mL batch reactor system (PARR Instruments). The reactor was equipped with a mechanical stirrer and a high stirring speed of 900 rpm and small catalyst particles (below 63 μm) were used in order to suppress the external and internal mass transfer limitations. The liquid samples were taken through a sampling line with specific time intervals. In a typical experiment 50 mg of the prereduced catalyst was added to the reactor system together with 50 mL of hexadecane and 100 mg of isoeugenol. All catalysts analyzed in this work were reduced ex-situ with a specific temperature program (Table S1) prior to HDO of isoeugenol. An 11

Table 1. Specific Surface Area, Pore Volume, Average Metal Particle Size for the Fresh and the Spent Catalysts, and Metal Dispersion Calculated from TEM Images

catalyst	metal loading (wt %)	specific surface area (m^2/g_{cat})	pore volume (cm^3/g_{cat})	avg metal diameter by XRD (nm)	avg metal diameter (nm)		TEM dispersion (%)
					fresh	spent	
20 wt % Ni/graphite	n.d.	204	0.42	10	6.1	7.8	16.4
11 w.% Ni/SiO$_2$	n.d.	244	0.51	11.6	9.7	10.1	10.3
10 wt % Co/SBA-15	16.4	471	0.62	n.d.	3.7	4.6	27.3
15 wt % Co/TiO$_2$	16.4[a]	94	0.19	n.d.	2.6	3.1	38.4
15 wt % Co/Al$_2$O$_3$	15.9[a]	203	0.55	6	3.3	3.4	30.2
11 w.% Co/SiO$_2$ (red. at 415 °C)	n.d.	203	0.55	n.d.	6.2	7.3	16.1
11 wt % Co/SiO$_2$ (red. at 550 °C)	n.d.	n.d.	n.d.	n.d.	5.9	7.8	16.9
SiO$_2$		378	0.72				
Al$_2$O$_3$		240					
SBA-15		650					
TiO$_2$		109					

[a]ICP method; n.d. not determined.

wt % Co/SiO$_2$ catalyst was also reused in hydrodeoxygenation of isoeugenol. Prior to its reuse the spent catalyst was washed with acetone and dried in air. Thereafter, it was calcined using the following temperature program: 5 °C/min to 100 °C then 2 °C/min to 415 °C (2 h) and prereduced prior to the first reuse in HDO of isoeugenol at 300 °C and 30 bar.

The liquid samples were analyzed by a gas chromatograph using a DB-1 capillary column (Agilent 122-103e, 30 m × 250 μm × 0.5 μm). The temperature program used for GC analysis was the following: 60 °C then 5 °C/min and 3 °C/min to 135 °C then 15 °C/min to 300 °C (1 min). The following chemicals were used to calibrate the GC method: isoeugenol (cis + trans) (≥98, Fluka), isoeugenol (cis + trans) (98%, Aldrich), dodecane (≥99% Alfa Aesar), n-hexadecane ≥99% Alfa Aesar, dihydroeugenol (≥99%, Sigma-Aldrich), 2-propanol (≥99.8, Sigma-Aldrich), benzene ≥99% Sigma-Aldrich, hexane (≥99%, Sigma-Aldrich), cyclohexane (99%, Lab Scan), heptane (≥99%, Sigma-Aldrich), 2-hexanol (99%, Aldrich), octane (≥99% Fluka), methoxycyclohexane (99%, Aldrich), propylcyclohexane (99% Aldrich), 4-propylphenol (99%, Sigma-Aldrich), and 1-decanol.

A gas sample of 0.5 mL was taken at 40 °C at the end of all HDO of isoeugenol experiments, using an Agilent 6890N-GC apparatus, with a GS-Q capillary column (30 m × 530 μm × 40 μm). The detection was done by a flame ionization detector (FID) at 300 °C to identify light hydrocarbon gases and a thermal conductivity detector (TCD) at 250 °C to identify gases containing oxygen. The following calibration gas mixtures were used: (1) 1.02 vol % methane, 1 vol % CO$_2$, 1 vol % ethylene, 0.972 vol % ethane, and rest helium supplied by AGA and (2) 1 vol % methane, 1 vol % ethane, 1 vol % propane, 1 vol % isobutane, 1 vol % n-butane (AGA).

Catalyst Characterization Methods. Liquid nitrogen physisorption was applied to determine the specific surface areas (SSAs) of the catalysts, using the Brunauer–Emmett–Teller (BET) method.[24] The measurements were done with a Carlo Erba Soptomatic 1900 apparatus. The buret, with the catalyst inside, after outgassing for 3 h at 150 °C, was placed in liquid nitrogen.

Fourier transform infrared (FTIR) spectroscopy (ATI Mattson FTIR) was used to measure Brønsted and Lewis acidity of the solid catalysts with pyridine as a probe molecule.[23] The catalyst was pressed into a thin wafer with a mass of 10−30 mg and then put into the FTIR cell. To determine the strength of acid site, pyridine was desorbed at 250, 350, and 450 °C for 1 h. Scanning was performed under vacuum conditions at 100 °C and spectral bands at 1545 and 1450 cm^{-1} were used to identify the Brønsted and Lewis acid sites, respectively. The amount of the acid sites was calculated using the molar extinction factor by Emeis.[25]

Temperature-programmed reduction by hydrogen (H$_2$-TPR) of unreduced catalysts using the same temperature program for reducing the catalyst as given in Table S1 (excluding 11 wt % Co/SiO$_2$ which was reduced at 415 °C) was used to find the most suitable reduction conditions for the catalysts used in HDO of isoeugenol. The analysis was done by a Micromeritics AutoChem 2910 instrument using a gas mixture composed of 5 vol % hydrogen in 95 vol % argon. The formed water was separated using a cold trap composed of a mixture of liquid nitrogen and 2-propanol. The catalysts analyzed by TEM and XRD were reduced at the same conditions as used for catalyst reduction prior to HDO of isoeugenol.

A transmission electron microscope (JEM-1400) was applied to analyze the metal particle distribution, metal particle size, and structure of the fresh and spent catalysts. The particle size distribution was calculated with the ImageJ software.

Thermogravimetric analysis (TGA) was used to follow the weight change of a catalyst by increasing the temperature in synthetic air. For Ni/graphite nitrogen atmosphere was used. TGA was done for both fresh and spent catalysts using a SDT Q600 V20.9 Build 20 instrument. The following temperature program was used: from 25 °C heating with a temperature ramp of 10 °C/min to 1000 °C using a gas flow rate of 100 mL/min.

CHNS analysis was performed with Thermo Fischer Scientific Flash 2000 Combustion CHNS/O apparatus to establish the content of carbon, hydrogen, nitrogen, and sulfur in the solid catalysts.

X-ray diffraction measurements were performed with Philips Empyrean diffractometer using Cu Kα radiation, Bragg−Brentano HD incident beam monochromator and a PiXcel 3DMedipix 3 detector. The samples were first ground to powder using a zero background silicon sample holder. Every measurement scanned the 2θ range from 5° to 100° with a step size of 0.0135° and a 40 s integration time per step. Different phases were identified using the HighScore program and Crystallography Open Database (COD). The particle sizes were determined using the Maud Rietveld refinement program.[26] The catalysts analyzed by XRD and TEM were prereduced at the same conditions as used for catalyst reduction prior to HDO of isoeugenol.

SEC analysis was performed with a SEC-HPLC equipped with two columns, a Guard column with the dimensions of 50 mm × 7.8 mm and a Jordi Gel DVB 500A column with the dimensions of 300 mm × 7.8 mm to investigate oligomers and polymers formation on the spent catalysts surface by extracting them from the spent catalysts with heptane.[27] For extraction 20 mg of spent catalysts was added to a round flask together with 20 mL of the solvent and a condenser. The flask was placed in an oil bath and heated to 98 °C, thereafter extraction occurred for 4 h with a stirring rate of 400 rpm. The flow

rate of the inert gas, consisting of 5% Ar in 95% N_2, was set to 100 mL/min. The solution obtained after the 4 h extraction was then kept at 40 °C until complete evaporation of heptane. The resulting residue was then dissolved in 10 mL of tetrahydrofuran (≥99.9%, Sigma-Aldrich), thereafter it was filtered for analysis. The resulting concentration of the residue was 2 mg/mL.

An apparatus consisting of a Zeiss Leo Gemini 1530 microscope together with detectors for backscattered and secondary electrons was used to identify the morphology of the catalysts.

Liquid samples obtained at the end of HDO of isoeugenol were analyzed with ICP-MS (equipment name) to study possible leaching of the metal into the liquid phase.

Definitions. The conversion was calculated according to eq 1

$$X_t(\%) = \frac{C_0 - C_i}{C_0} \times 100\% \tag{1}$$

where X_t is conversion at time t, C_0 initial molar concentration (mol/L) of isoeugenol, and C_i is the molar concentration of isoeugenol at time t. The sum of the liquid phase compounds visible in GC was calculated with the following formula 2:
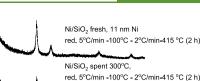
$$GCLPA (\%) = \frac{GCLPA_t}{GCLPA_0} \times 100\% \tag{2}$$

With $GCLPA_t$ being the sum of the masses of reactants and products obtained in GC at time t and $GCLPA_0$, the initial sum of reactants and products (eq 2) without the gas phase products (e.g., methane, ethane, ethylene, propane, butane, and isobutene) and compounds adsorbed on the catalyst surface (i.e., strongly adsorbed species, oligomers, and polymers), meaning that the GCLPA does not reflect the full mass balance of the reaction.

■ RESULTS AND DISCUSSION

Catalyst Characterization Results. The measured Co loading in 15 wt % Co/TiO$_2$ and 15 wt % Co/SiO$_2$ were close to the nominal ones (Table 1). The specific surface areas (SSA) and their respective pore volumes differ from 94−471 m^2/g and from 0.19−0.62 cm^3/g, respectively for the catalysts used in HDO of isoeugenol. The highest specific surface area obtained for 10 wt % Co/SBA-15 is in line with previous measurements reported in literature.[28] For 11 wt % Co/SiO$_2$ and 11 wt % Ni/SiO$_2$, it should be mentioned that the SSA were affected by the preparation method and that the SSA of the catalysts prepared by impregnation with Co and Ni exhibit lower specific surface area of the supports as reported in ref 29. The original SSA for SiO$_2$ was 378 m^2/g$_{cat}$ with the pore volume of 0.72 cm^3/g$_{cat}$ indicating that SSA was 54 and 65% from the original SSA of the support, for Co and Ni supported on SiO$_2$, respectively. Lower values of surface areas as expected were observed for other supported catalysts materials in comparison with the pristine supports.

XRD results of Ni- and Co-based catalysts are shown in Figure 2 and Table 1. XRD results for 11 wt % Ni/SiO$_2$ showed a large peak at 45° that can be identified as metallic Ni(111) and three smaller peaks at 50°, 78°, and 95° related to Ni phases.[30] The Ni crystal size was calculated according to the Rietveld refinement to be 11.6 nm and corresponds quite well to the metal crystal size determined by TEM (Table 1). For Ni/graphite XRD showed a rather similar crystal size of 10 nm, as for Ni/SiO$_2$. For the fresh 10 wt % Co/SBA-15, 11 wt % Co/SiO$_2$ reduced at 415 °C as well as for 11 wt % Ni/SiO$_2$ an amorphous phase was identified at 20° (Figure S1).[31] It is worth mentioning that the signals for cobalt peaks were too small for 11 wt % Co/SiO$_2$ reduced at 415 °C most probably due to the small size of cobalt not visible by XRD (Table 1),
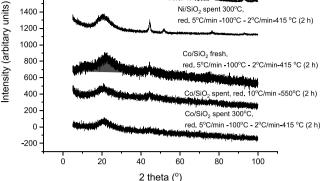
Figure 2. XRD results of the fresh and spent catalysts.

even if according to TEM showed the average particle size of Co is 6.2 nm.

The cubic cobalt phase was present in both 10 wt % Co/SBA-15 and 15 wt % Co/Al$_2$O$_3$. According to Rietveld analysis the cell parameter for Co was higher, 3.53 Å[32] in 10 wt % Co/SBA-15 than in the 15 wt % Co/Al$_2$O$_3$ which had a cell parameter of 3.51 Å. The diffractogram for 15 wt % Co/Al$_2$O$_3$ shows metallic cobalt with a size of 7 nm and the presence of the hexagonal form of corundum at 40° (Figure S3). The 15 wt % Co/TiO$_2$ shows peaks at approximately 22°, 30°, 38°, 50° and some smaller peaks between 60° and 90° (Figure S3). This catalyst exhibits peaks from cobalt oxides species, Co$_2$O$_3$ with a size of ca. 21 nm together with the peak at approximately 25° confirming the TiO$_2$ anatase structure.[33] The titania support in 15 wt % Co/TiO$_2$ has a small specific surface area (Table 1) and gives larger metal oxide crystal sizes than other catalysts.

TEM images and histograms for all catalysts are shown in Figures 3−7 and S2−S3. The metal dispersion for the fresh catalysts (Table 1) was calculated according to

$$\frac{1 \text{ nm}}{\text{avg } d(\text{nm})} \times 100 = D(\%) \tag{3}$$

TEM results (Figure 3) of 20 wt % Ni/graphite, both fresh (A) and spent (B), as well as their respective histograms of metal particle size diameter of the fresh 20 wt % Ni/graphite (A) was calculated to be 6.1 nm. Nevertheless, some particles are above 15 nm in diameter, indicating a considerable spread in the metal particle size distribution. The histogram of the spent 20 wt % Ni/graphite (B) shows a small increase in average metal particle diameter after HDO of isoeugenol indicating some metal sintering during the reaction (Figure 3B). This is due to weak interaction between graphite and nickel.

TEM images of the fresh and the spent 11 wt % Ni/SiO$_2$ (Figure 4) show that the size of Ni particles varies in the range of 9−50 nm, with the average metal particle diameter being 9.7 nm for the fresh catalyst and 10.1 nm for the spent one. Ni/graphite exhibited slightly smaller particles in comparison to 11 wt % Ni/SiO$_2$ despite its small specific surface area (Table 1).

The porous structure of the support is clearly visible for 11 wt % Co/SiO$_2$ reduced at 415 °C in Figure 6A, with metal particles located close to each other in larger agglomerates. The metal particle size varies from smaller particles of 3 nm to larger ones of the size 100 nm. The TEM image of the spent 11 wt % Co/SiO$_2$ reduced at 415 °C shows a large dark area in the bottom left corner that can be identified as coke (Figure
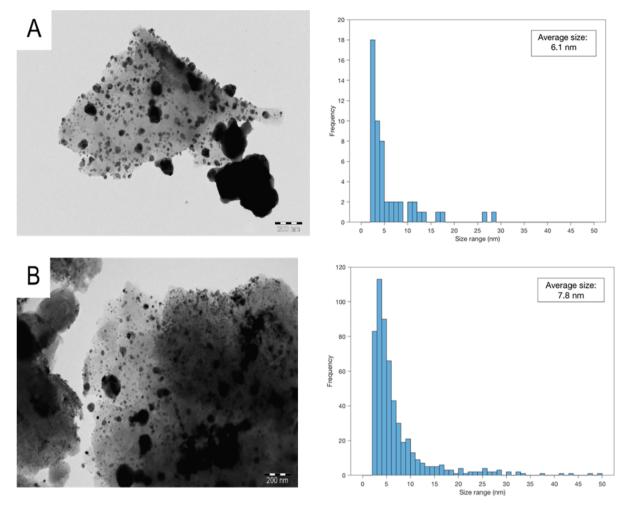
Figure 3. TEM images and histograms of the fresh (A) and the spent (B) 20 wt % Ni/graphite in HDO of isoeugenol. The scale bar is 200 nm.

6B). Moreover, an increase in the metal particle diameter (Table 1) indicates that minor sintering occurs since cobalt and SiO_2 have weak interactions.[34] In addition, the particle size for 11 wt % Co/SiO_2 is smaller than for 11 wt % Ni/SiO_2. The change in the reduction temperature for 11 wt % Co/SiO_2, reduced either at 415 or 550 °C did not affect the metal particle size very much. Only a slight increase in the metal particle size can be seen after HDO of isoeugenol at 300 °C under 30 bar hydrogen for 11 wt % Co/SiO_2 reduced at 550 °C, increasing from 5.9 to 7.8 nm. It can be concluded that sintering is not prominent for these catalysts under the studied reaction conditions.

The channels with the diameter of 10 nm in the TEM image of 10 wt % Co/SBA-15 (Figure 5) are visible similar to reported in the literature.[35] Although large metal particles can be seen for the fresh and spent 10 wt % Co/SBA-15 catalysts varying from 50 to above 150 nm, the average metal particle size diameter of the fresh and spent 10 wt % Co/SBA-15 is small, 3.7 and 4.6 nm, respectively.

A TEM image of the fresh 15 wt % Co/TiO_2 shows a narrow spread in the metal particle size, ranging from 1−8 nm (Figure S1). The average metal particle size diameter increased to 3.1 nm for the spent 15 wt % Co/TiO_2 compared to 2.6 nm for the fresh 15 wt % Co/TiO_2. On the other hand, large agglomerates can be seen for 15 wt % Co/Al_2O_3, appearing as smaller particles are also close to each other giving a small average metal particle size (Table 1, Figure S2). The

histograms of 15 wt % Co/Al_2O_3 show only a minimal increase in the average metal particle diameter, indicating absence or negligible sintering. The reason for this can be strong interactions between cobalt and the support.[36]

The pyridine-FTIR results show that only 15 wt % Co/Al_2O_3 has weak Brønsted acid sites as well as weak and medium Lewis sites (Table 2). The other two catalysts, 10 wt % Co/SBA-15 and 15 wt % Co/TiO_2, display also the presence of a minor amount of weak Lewis acid sites. The 15 wt % Co/TiO_2 catalyst was the most acidic, while 11 wt % Co/SiO_2 reduced at 415 and 550 °C did not show acidity.

The H_2-TPR results show both the reduction program as well as the hydrogen consumption (Figure 8, Table 3). The relative hydrogen consumption decreased in the following order: 11 wt % Co/SiO_2 > 11 wt % Ni/SiO_2 > 10 wt % Co/SBA-15 > 15 wt % Co/Al_2O_3 confirming that less cobalt on Al_2O_3 is reduced due to strong interactions with the support and the maximum reduction temperature is higher. Although the Co metal particle size was small in Co/Al_2O_3, the hydrogen consumption was low indicating that not all Co is reduced to the metallic form under these conditions. The interactions between CoO and alumina are the strongest resulting in the formation of an inactive Co−Al spinel; therefore, 15 wt % Co/Al_2O_3 has the lowest reducibility, and thus, the highest content of the metal is needed for catalytic activity.[37,38]

For 11 wt % Ni/SiO_2 it can be seen that NiO was reduced at high temperature, approximately 380 °C (Figure 8a). The
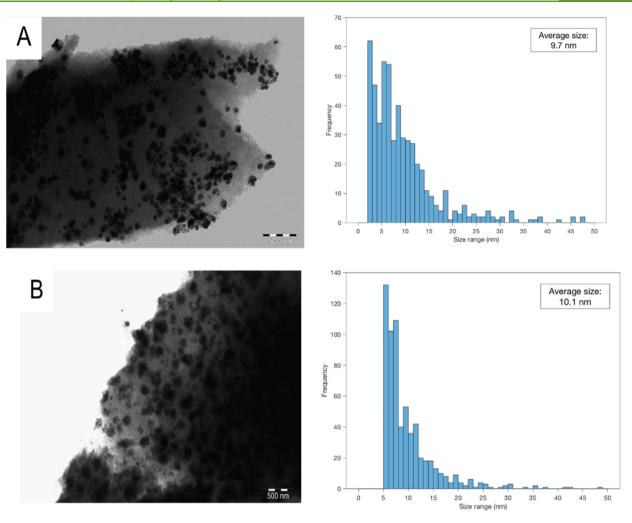
Figure 4. TEM images and histograms of the fresh (A) and the spent (B) 11 wt % Ni/SiO_2. The scale bar is 500 nm.

relative hydrogen consumption for this catalyst was, however, the second largest one (Table 3) due to relatively large metal particles on SiO_2, which are easy to reduced (Table 1).

On the other hand, hydrogen consumption for 10 wt % Co/SBA-15 and for 11 wt % Co/SiO_2 starts already at a relatively low temperature (Figure 8b and d, Table 3). TPR for 11 wt % Co/SiO_2 treated at 415 °C shows a broad peak split in two parts in the interval of 350−415 °C. Reduction of Co_3O_4 to Co^0 occurs according to H_2-TPR data in this work and according to the literature in two steps:[39]

$$Co_3O_4 + H_2 \rightarrow 3CoO + H_2O \qquad (4)$$

$$CoO + H_2 \rightarrow Co + H_2O \qquad (5)$$

It has been reported[40] that reduction of CoO to metallic Co occurs at 400 °C. A large, narrow peak at 40 min corresponding to 420 °C is visible for Co/SBA-15 when Co has weak interactions with the support. This is most likely due to reduction of Co_3O_4 to CoO and CoO to metallic Co happening simultaneously, due to strong interactions between the support and cobalt oxides.[37]

Organic residue and coke were analyzed in the spent catalysts by several methods, e.g. by TGA, CHNS analysis, and extracting the spent catalyst with heptane and analyzing by size exclusion chromatography (SEC). TGA results were evaluated by excluding water at 100 °C and comparing the weight losses of both the fresh and the spent samples, while the amount of

coke was calculated by subtracting the weight loss of the fresh catalyst in the temperature range of 100−1000 °C from that of the spent catalyst. The results showed that coking is on a similar level (22−25%) for Ni/graphite, Ni/SiO_2, and Co/SiO_2. The lowest coking is observed for 15 wt % Co/Al_2O_3 (Table 4) which is interesting considering that 15 wt % Co/Al_2O_3 is the only acidic one (Table 2) thus higher coke formation could be anticipated.[41] The low organic coke percentage for 15 wt % Co/Al_2O_3 was in line with a larger formation of gases, as can be seen in gas phase analysis results discussed below. The mass losses in the fresh and the spent 15 wt % Co/Al_2O_3, Co/SiO_2, and Ni/SiO_2 at ca. 150−200 °C show (Figure S4, Table 4) removal of lighter hydrocarbons, which correspond to soluble soft coke. The main weight loss for Ni/graphite occurred at a higher temperature, between 200 and 370 °C in nitrogen (Figure S4a). Higher molecular derivatives[42] and solid oxygenated compounds[43,44] are proposed to be formed from soluble carbon for 11 wt % Ni/SiO_2 and 11 wt % Co/SiO_2 (Figure S3b−d).

All spent catalysts analyzed with CHNS exhibited a molar ratio of H/C higher than 2, indicating that the coke present in the catalysts is not of aromatic nature.[45] The spent catalysts also contain a relatively high amount of carbon, ranging from 16 to 26%, the highest being for 11 wt % Ni/SiO_2 followed by 24% over 11 wt % Co/SiO_2 and 17% for 15 wt % Co/Al_2O_3.
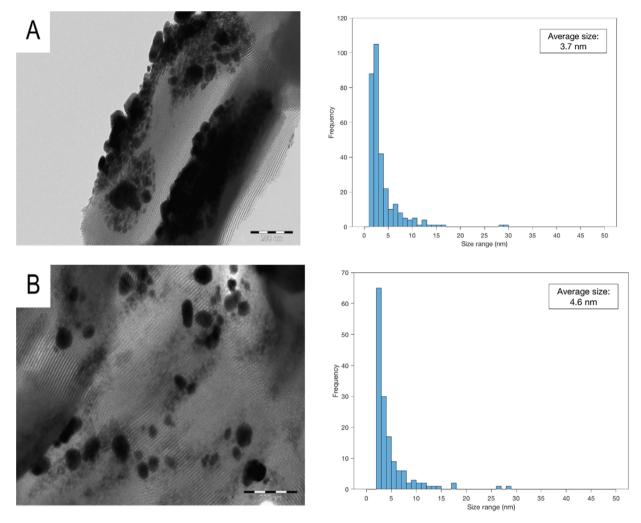
Figure 5. TEM images and histograms of the fresh (A) and spent (B) 10 wt % Co/SBA-15 in HDO of isoeugenol. The scale bar is 200 nm.

Interestingly, the reused 11 wt % Co/SiO$_2$ reduced at 415 °C shows much lower carbon content than 11 wt % Co/SiO$_2$.

SEC analysis performed only for the spent 15 wt % Co/Al$_2$O catalysts revealed that it contained high molecular weight compounds compared to the reference sitosterol (415 g/mol) (Figure S5, Tables S2−S3). These compounds can be easily removed in TGA having nonaromatic according to EDXA analysis.

ICP-MS results for the liquid samples obtained at the end of HDO of isoeugenol experiments (Table S3) did not demonstrate any leaching, except an experiment with 11 wt % Ni/SiO$_2$ showing minor traces of silicon.

Isoeugenol HDO. Two different Ni-based catalysts, namely 20 wt % Ni/graphite and 11 wt % Ni/SiO$_2$, and four different supported Co-catalysts, 11 wt % Co/SiO$_2$, 15 wt % Co/Al$_2$O$_3$, 10 wt % Co/SBA-15, 15 wt % Co/Al$_2$O$_3$, and 15 wt % Co/TiO$_2$, were investigated in isoeugenol HDO (Table 5 and Figures 9−14). Over Ni-supported catalysts, isoeugenol was reacting very fast to dihydroeugenol (DH) already during heating the reactor to the desired temperature in the absence of stirring in a stainless steel autoclave as reported earlier[14] and its conversion was complete in 1 min.

The sum of the reactant and product masses visible in GC analysis (GCLPA), including, along with aromatic and cyclic products also hexane and heptane originating from isoeugenol, was high (86%) for 20 wt % Ni/graphite at 200 °C with dihydroeugenol as the main product (Table 5). At 300 °C, the GCLPA levels were lower (70%) than at 200 °C due to more extensive HDO. In addition, 11 wt % Ni/SiO$_2$ gave lower GCLPA than 20 wt % Ni/graphite due to its higher HDO activity (Table 5). Because of different metal loadings, the yields of DH are compared at the normalized time 1.0 min*g$_{Ni}$ (Table 5). The results showed that Ni/graphite produced mainly DH at 200 °C and deoxygenation was not efficient under these conditions opposite to Pt supported on Beta zeolites.[13]

Upon temperature elevation to 300 °C for these nonacidic Ni supported catalysts (Table 5, entries 2 and 3) the formed dihydroeugenol was rapidly reacting further to propylcyclohexanone (Figure 9a, b) and further to 3-,4-propylcyclohexane and propylcyclohexane (Figures 9c, d). It is also noteworthy that despite the better nickel dispersion in 20 wt % Ni/graphite in comparison to 11 wt % Ni/SiO$_2$ (Table 1), the former was not efficient in HDO. Comparison of the product distribution in HDO of isoeugenol over 20 wt % Ni/graphite and 11 wt % Ni/SiO$_2$ shows propylcyclohexanone (PCHone) disappeared more slowly with Ni/SiO$_2$ before 0.5 min*g$_{cat}$ normalized time than with Ni/graphite (Figure 9b), while the yields of PCHone were the same over these catalysts at 1.0 min*g$_{cat}$ (Table 5). This intermediate is formed via keto−enol tautomerization from a partially hydrogenated propylcyclohexenol. Propylcyclohexanone is further hydrogenated to propylcyclohexanol.
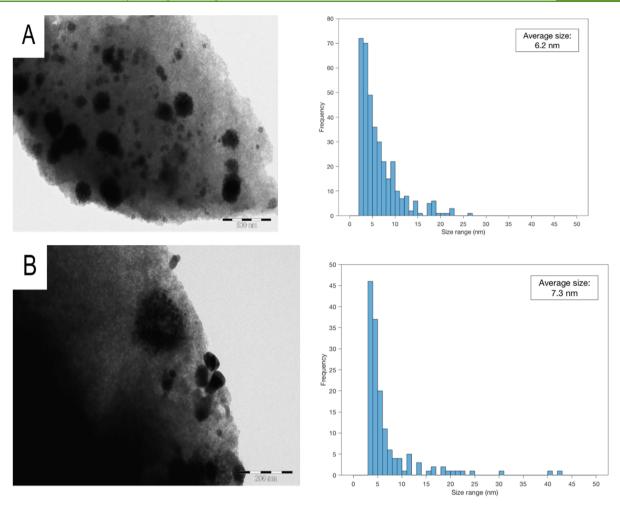
Figure 6. TEM images and histograms of the fresh (A) and the spent (B) 11 wt % Co/SiO$_2$ reduced at 415 °C in HDO of isoeugenol. The scale bar for (A) is 500 nm and for (B) is 200 nm.

The latter undergoes dehydration to propylcyclohexene, and subsequent hydrogenation to propylcyclohexane. When plotting the concentration of propylcyclohexene vs concentration of propylcyclohexane (Figure 9d), it can be seen that over 11 wt % Ni/SiO$_2$ hydrogenation of propylcyclohexene occurs slower than over 20 wt % Ni/graphite in line with its lower dispersion correlating with lower hydrogenation ability. In order to compare the performance of catalysts bearing different metal particle sizes at the same conversion level, the yields of 3-,4-propylcyclohexene, propylcyclohexane, and cyclohexene were compared at 50% conversion of dihydroeugenol. It should be noted, as earlier stated, that because isoeugenol is converted very rapidly, the yields of different products could not be correlated with its conversion. The results display (Table 5, Figure 11) that the first product formed from dihydroeugenol and visible in GC, i.e. 3-,4-propylcyclohexene, was formed in about the same yields over Ni/G and Ni/SiO$_2$ catalysts despite their different metal particle sizes (Figure 11a). The cluster sizes were, however, quite large, 6 and 10 nm. The same is valid for the yields of propylcyclohexane (Figure 11b), while 11 wt % Ni/SiO$_2$ gave a much higher yield of cyclohexene than 20 wt % Ni/G (Figure 11c). The yield of the main desired product, propylcyclohexane was 60% after 4 h over 20 wt % Ni/graphite (Table 5, Figure 9c), which is in accordance with its relatively high metal dispersion and Ni loading,[46] facilitating hydrodeoxygenation.

As a comparison with the literature,[21] 98% selectivity to propylcyclohexane at complete eugenol conversion was obtained over 10 wt % Ni-sulfated zirconia at 300 °C under 50 bar hydrogen in 8 h. The NiO particle size in this catalyst determined by XRD was 12.1 nm. This result is in line with the current work. In addition, 10 wt % Ni/SBA-15 afforded 75% yield of propylcyclohexane in isoeugenol HDO at 300 °C under 30 bar of total pressure,[18] while in the current case it was 44% over 11 wt % Ni/SiO$_2$. In the former case, the Ni particle size was rather large 20 nm, which can be explained by the incipient wetness impregnation method and reduction after calcination using the following temperature program: 10 °C/min to 350 °C for 3 h.[18] In the current case the Ni particle size was 9.7 nm due to impregnation in an aqueous solution and applying a very slow temperature increase during catalyst reduction, 2 °C/min up to 415 °C for 2 h. This comparison shows that a lower yield of propylcyclohexane was obtained with the latter catalyst containing smaller Ni particles. Furthermore, smaller Ni particles in Ni/SiO$_2$ deactivated faster than larger ones in Ni/SBA-15 because complete conversion of dihydroeugenol and less intermediate products was observed in ref 18 in comparison to the current work.

The largest difference in the product distribution between Ni/SiO$_2$ and Ni/graphite catalysts is a higher yield of cyclohexene obtained at 1.0 min*g$_{Ni}$ normalized time over 20 wt % Ni/graphite. Cyclohexene yield, however, decreased
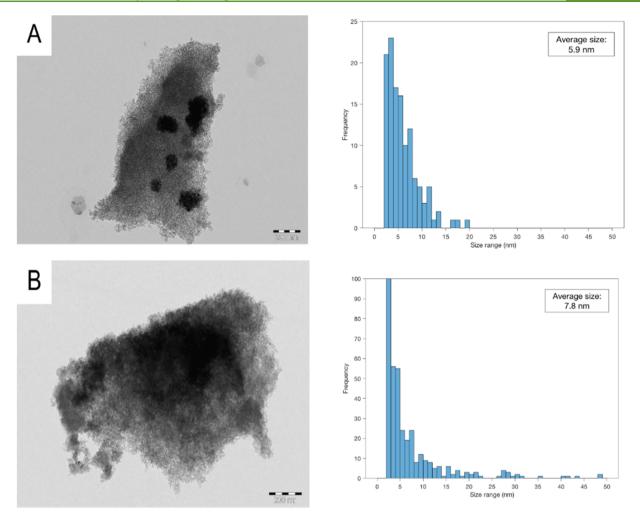
Figure 7. TEM images and histograms of the fresh (A) and the spent (B) 11 wt % Co/SiO$_2$ reduced at 550 °C in HDO of isoeugenol. The scale bar is 200 nm.

Table 2. Quantification of Brønsted and Lewis Acid Sites

	Brønsted acid sites (μmol/g)			Lewis acid sites (μmol/g)		
catalyst	250 °C	350 °C	450 °C	250 °C	350 °C	450 °C
20 wt % Ni/ graphite		n.d.[a]			n.d.	
11 wt % Ni/SiO$_2$	0	0	0	0	0	0
10 wt % Co/ SBA-15	0	0	0	2	0	0
15 wt % Co/ TiO$_2$	0	0	0	123	0	0
15 wt % Co/ Al$_2$O$_3$	3	0	0	25	3	0
11 w.% Co/SiO$_2$	0	0	0	0	0	0

[a]Not determined.

during increasing reaction time (Table 5, entry 2,3). It should be noted that Ni/SiO$_2$ is a nonacidic catalyst and the hydrogenolysis activity is thus related to properties of Ni. The results from the gas phase analysis can partially explain a decrease of the cyclohexene yield with prolonged reaction times. The 20 wt % Ni/graphite catalyst produced a more than double amount of gaseous products in comparison with 11 wt % Ni/SiO$_2$. The reason for this behavior is a high metal loading for the former catalyst, as nickel is known to form large amounts of methane in HDO of phenolic compounds.[47]

Propylcyclohexane yield with 10 wt % Co/SBA-15 was 63% after 4 h, higher than for 20 wt % Ni/graphite.

Four different Co supported catalysts were compared in HDO of isoeugenol at 200 and 300 °C (Figure 10a). In addition a blank experiment in the absence of isoeugenol was performed over 15 wt % Co/Al$_2$O$_3$ in order to observe if the solvent, hexadecane, undergoes cracking over this catalyst. The blank experiment revealed that no reaction occurred indicating that the observed hexane and heptane are formed exclusively from isoeugenol over Ni- and Co-supported catalysts. This result is different from reported previously in ref 14 with Ir–Re/Al$_2$O$_3$ catalyst.

The lowest GCLPA was obtained with 15 wt % Co/TiO$_2$ displaying Lewis acidity followed by 15 wt % Co/Al$_2$O$_3$ (Table 5). The latter one promoted methane and oligomer formation as described in more detail.

The slowest initial transformation of DH was observed over Co/TiO$_2$ followed by Co/Al$_2$O$_3$, which was about half of the rate observed for 10 wt % Co/SBA-15, while the highest rate was determined for 11 wt % Co/SiO$_2$ being 2 fold that of 11 wt % Co/SBA-15. This order for transformation of DH is not directly related to the metal dispersion (Table 1). A high catalytic activity of 11 wt % Co/SiO$_2$ can be correlated to its largest hydrogen consumption in TPR (Table 3). Table 5
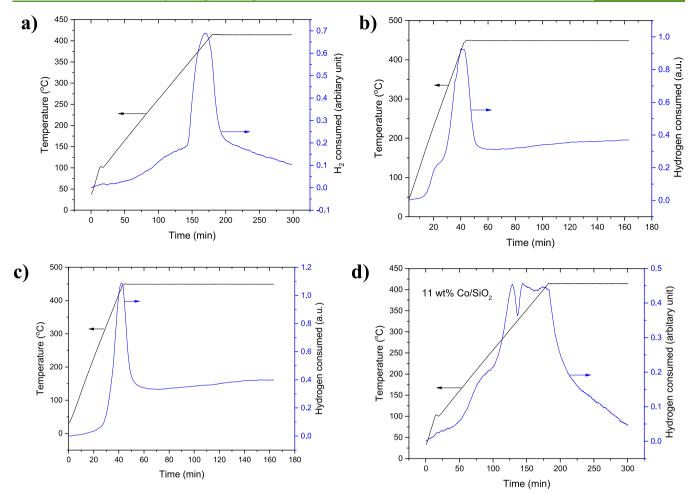
Figure 8. H$_2$-TPR of (a) 11 wt % Ni/SiO$_2$, (b) 10 wt % Co/SBA-15, (c) 15 wt % Co/Al$_2$O$_3$, (d) 11 wt % Co/SiO$_2$ (reduced at 415 °C).

Table 3. H$_2$-TPR Results of Different Catalysts

catalyst	relative area	T_{max} (°C)
11 wt % Ni/SiO$_2$	4.7	380
10 wt % Co/SBA-15	1.6	260, 420
15 wt % Co/Al$_2$O$_3$	1	410
11 wt % Co/SiO$_2$ (415 °C)	5.4	210, 300

Table 4. Total Coke Content Determined by TGA and CHNS Analysis in the Catalysts Used in HDO of Isoeugenol

catalyst	organic coke (N$_2$), %	organic coke (air), %	coke by CHNS (%)
20 wt % Ni/graphite	22.4	n.d.[a]	n.d.
11 wt % Ni/SiO$_2$	n.d.	25.0	26
11 wt % Co/SiO$_2$	n.d.	23.8	24
15 wt % Co/Al$_2$O$_3$	n.d.	28	17

[a]Not determined.

confirms that HDO proceeded much faster over this catalyst at a higher temperature.

Comparison of the product distribution with Co based catalysts (Figure 10) showed that rapid hydrogenation of the phenyl ring occurred forming first propylcyclohexenol. This enol was not observed at all since it was instantaneously converted to a corresponding ketone—propylcyclohexanone. The latter then reacts to propylcyclohexanol with subsequent dehydration to propylcyclohexene and hydrogenation to propylcyclohexane. The yields of propylcyclohexane decreased in the following order: Co/SBA-15 > Co/SiO$_2$ > Co/Al$_2$O$_3$ > Co/TiO$_2$ (Figure 10c). Cobalt and nickel supported on silica were slightly less efficient catalysts for deoxygenating propylcyclohexanone at the normalized time 1.0 min*g$_{metal}$ than Ni supported catalysts (Table 5). Furthermore, the concentration of propylcyclohexanone remained constant for Co/TiO$_2$ indicating its partial deactivation (Figure 10b). It is also noteworthy that the rate for formation of propylcyclohexane was very low over an acidic Co/Al$_2$O$_3$. Deactivation of Co/Al$_2$O$_3$ can be caused by the presence of large oligomers on the catalyst surface confirmed by SEC analysis (Figure S5, Tables S2−S3). When the concentration of propylcyclohexene is plotted vs the concentration of propylcyclohexane (Figure 10d) it can be observed that the ratio between the formation rates of propylcyclohexene to propylcyclohexane was 7 fold higher for 11 wt % Co/SiO$_2$ in comparison to 10 wt % Co/SBA-15 (Figure 10d). Fast disappearance of propylcyclohexene was observed over Co/Al$_2$O$_3$ and Co/TiO$_2$.

Highly dispersed Co particles in 15 wt % Co/TiO$_2$ and 15 wt % Co/Al$_2$O$_3$ facilitated rapid hydrogenation of propylcyclohexene to propylcyclohexane, which is shown in Figure 11c as a low yield of propylcyclohexene (Figure 11a, b), when comparing the yields of 3-,4-propylcyclohexene, propylcyclohexane, and cyclohexene at 50% conversion level of dihydroeugenol as a function of Co-particle size. A 15 wt % Co/TiO$_2$ catalyst gave also a low yield of cyclohexene due to

Table 5. Experimental Results from Isoeugenol HDO under 30 bar Hydrogen[a]

entry	catalyst	T (°C)	GCLPA (%)[b]	DH yield (%)[c,d]	PCHone yield (%)[c,d]	PB yield (%)[c,d]	3-,4-PCHENE yield (mol-%)[c,d]	PCH yield (mol-%)[c,d]	C-ENE yield (%)[c,d]
1	20 wt % Ni/graphite	200	86	86[c] (83[d])	0[c] (0[d])	0[c] (0[d])	<1[c] (1.5[d])	0[c] (0[d])	<1[c] (<1[d])
2	20 wt % Ni/graphite	300	73	17[c] (2[d])	4[c] (2[d], 6[e])	0[c] (0[d], 0[e])	4[c] (2[d],13[e])	35[c] (60[d], 10[e])	9[c] (1[d], 1[e])
3	11 w.% Ni/SiO$_2$	300	70	5[c] (1[d])	4[c] (3[d], 6[e])	<1[c] (<1[d], <1[e])	10[c] (6[d], 14[e])	33[c] (44[d], 10[e])	5[c] (3[d], 7[e])
4	10 wt % Co/SBA-15	200	93	86[c] (80[d])	0[c] (0[d])	0[c] (0[d])	4[c] (6[d])	0[c] (0[d])	1[c] (2[d])
5	10 wt % Co/SBA-15	300	79	2[c] (1[d])	0[c] (0[d], 7[e])	0[c] (0[d], 0[e])	3[c] (1[d], 18[e])	58[c] (63[d], 19[e])	1[c] (<1[d], 8[e])
6	15 wt % Co/TiO$_2$	300	38	31[c] (13[d])	3[c] (2[d], 3[e])	0[c] (0[d], 0[e])	2[c] (1[d], 2[e])	4[c] (9[d], 4[e])	1[c] (<1[d], 1[e])
7	15 wt % Co/Al$_2$O$_3$	300	56	4[c] (0[d])	0[c] (0[c], 0[c])	0[c] (0[d], 0[e])	<1[c] (<1[d], <1[e])	25[c] (10[d], 24[e])	<1[c] (2[d], 0[e])
8	11 w.% Co/SiO$_2$ (415 °C)	200	87	84[c] (74[d])	0[c] (0[c])	0 (0[c])	5 (10[c])	0 (0[c])	2 (4[c])
9	11 w.% Co/SiO$_2$ (415 °C)	300	73	4[c] (3[d])	5[c] (4[d], 8[e])	<1[c] (0[d],0[e])	9[c] (5[d], 32[e])	43[c] (50[d], 4[e])	4[c] (2[d], < 1[e])
10	11 w.% Co/SiO$_2$ (550 °C)	300	73	6[c] (2[d])	5[c] (4[d], 7[e])	2[c] (0.8[d], 2[e])	10[c] (5[d], 18[e])	38[c] (50[d], 17[e])	5[c] (2[d], 8[e])

[a]Notation: DH dihydroeugenol, PB propylbenzene, PCH propylcyclohexane, C-ENE cyclohexene, PCHone propylcyclohexanone, 3-,4-PCHENE propylcyclohexene. [b]Sum of the masses of reactant and products in liquid phase determined by GC (%) at 60% conversion. [c]Yield at 1.0 min*g$_{metal}$ normalized time. [d]Yield after 240 min in parentheses. [e]Yield at 50% conversion of dihydroeugenol.
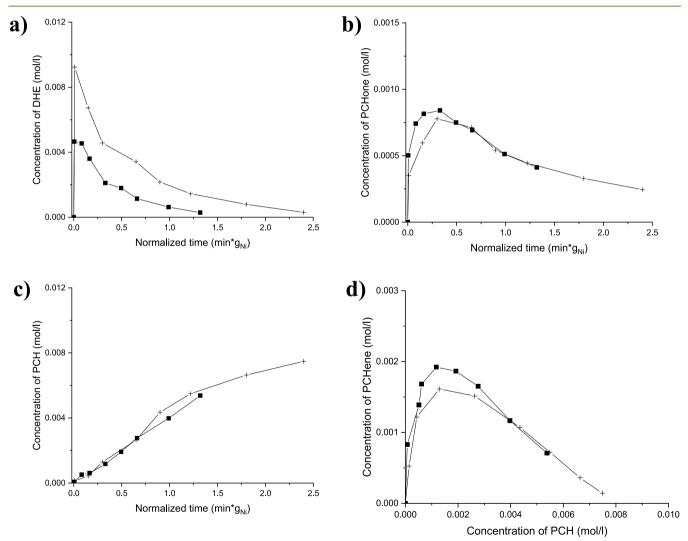

Figure 9. Molar concentration of (a) dihydroeugenol and (b) propylcyclohexanone, (c) propylcyclohexane vs reaction time, and (d) propylcyclohexene concentration as a function of the concentration of propylcyclohexane for 11 wt % Ni/SiO$_2$ (■) and 20 wt % Ni/G (+) in HDO of isoeugenol at 300 °C under 30 bar hydrogen.

its high dispersion and resulted in the lowest GCLPA (Figure 11c, Table 5). A complex reaction network involving a sequence of steps (hydrogenation of the phenyl ring; keto−enol tautomerization, hydrogenation of the keto-group,
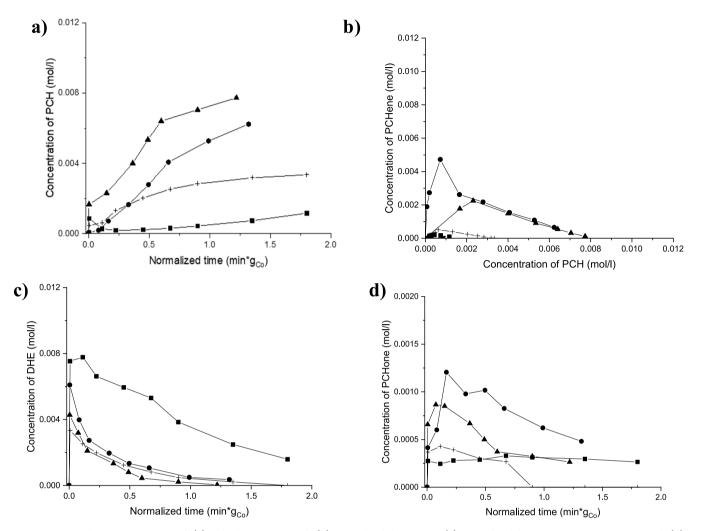
Figure 10. Molar concentration of (a) dihydroeugenol and (b) propylcyclohexanone, (c) propylcyclohexane vs reaction time, and (d) propylcyclohexene concentration as a function of the concentration of propylcyclohexane for 10 wt % Co/SBA-15 (▲), 11 wt % Co/SiO₂ (●), 15 wt % Co/TiO₂ (■), and 15 wt % Co/Al₂O₃ (+) in HDO of isoeugenol.

dehydration, hydrogenation of the olefinic group) requires different types of sites, thus the catalytic results cannot be explained exclusively just by one single parameter related to hydrogenation ability, e.g. metal dispersion.

The results from gas phase analysis in HDO of isoeugenol showed that methane was the most prominent gaseous product over all catalysts (Figure 11). The area of methane formed over Ni/graphite in HDO of isoeugenol at 300 °C under 30 bar was 2.1 fold higher than for Ni/SiO₂ (Figure 11). When, however, dividing the methane area obtained by these catalysts, by the moles of surface Ni based on TEM (Table 1), the normalized area of methane after 240 min per exposed Ni was 1.4 higher for Ni/SiO₂ than for Ni/graphite. The cyclohexene yields and GCLPA levels after 240 min or 20 wt % Ni/graphite and for 11 wt % Ni/SiO₂ were 1% and 3% and 73% and 70%, respectively (Table 5), thus showing the link between methane and cyclohexene formation as well as lower GCLPA observed over 10 wt % Ni/SiO₂. These results clearly show the link between the yield of cyclohexene and formation of methane, because gaseous products are formed when propylcyclohexene is decomposed (Figure 1). Noteworthy is also that over the acidic 15 wt % Co/Al₂O₃, 13-fold more methane was formed

in comparison to the second most active catalyst for methanation, i.e. Co/SiO₂ (415 °C). A high amount of gaseous products formed for 15 wt % Co/Al₂O₃ can further be explained by its high metal loading as well as by low amount of organic coke indicated by TGA (Table 4). The latter observation is interesting, as acidic supports tend to form coke in HDO reactions,[41] which is not the case here. The highest relative amount of ethane was also obtained with Co/Al₂O₃ catalyst, being 6.6 fold that obtained over Co/SiO₂ (550 °C). It is also important to note that nearly a double amount of methane was formed over Co/SiO₂ (415 °C) in comparison to Ni/graphite, over which the methane amount was the third highest. Other formed gaseous products were propane, butane and isobutane, while the relative amounts of ethylene were rather small.

Effect of the initial concentration of isoeugenol was investigated using 0.012 and 0.1 mol/L isoeugenol with the same reactant to 11 wt % Co/SiO₂ mass ratio of 2 (Figure 13). The GCLPA for the initial reactant concentration of 0.1 mol/L dropped very fast to 46% and remained constant during the reaction, while it was 72% in the HDO of isoeugenol with the initial isoeugenol concentration 0.012 mol/L. This result
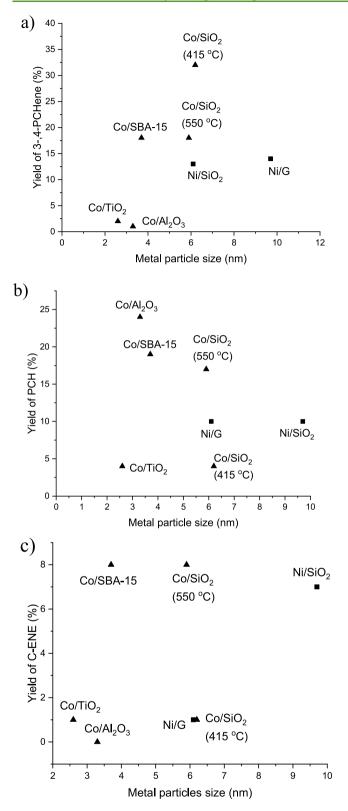
Figure 12. Intensities of different gaseous products in the chromatogram obtained from HDO of isoeugenol at 300 °C under 30 bar hydrogen over all catalysts, except Co/TiO$_2$, for which gaseous products were not analyzed.

Figure 13. Molar concentration of dihydroeugenol and propylcyclohexanone as a function of time for 11 wt % Co/SiO$_2$ in HDO of isoeugenol. Symbols: the initial isoeugenol concentration of 0.012 mol/L (open symbol), 0.1 mol/L (solid symbol), dihydroeugenol (■), propylcyclohexane (●). The ratio of the mass of isoeugenol to mass of catalyst is 2.

Figure 11. Yield of (a) 3-,4-propylcylohexene, (b) propylcylohexane, and (c) cyclohexene at 50% conversion of dihydroeugenol as a function of metal particle size. Notation: (■) Ni catalysts and (▲) Co catalysts.

indicates strong adsorption of the reactant on the catalyst surface. Although formation of dihydroeugenol was higher for a more concentrated isoeugenol, the rate at which dihydroeugenol reacted further was only 30% of the rate
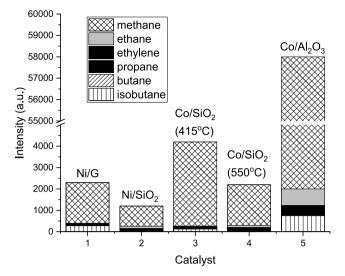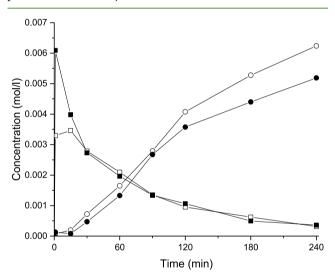
observed for the more diluted solution. This result is opposite to the one the authors have previously found for Ir–Re/Al$_2$O$_3$ catalyst, for which the first order kinetics was observed.[14] In the current work using different concentrations of isoeugenol, dihydroeugenol reacted further and catalysts retained their activity. Formation of propylcyclohexane was more prominent in more diluted solution indicating some catalyst deactivation and formation of more propylbenzene in a more concentrated solution. The presence of propylbenzene (not shown), which was visible among the products at 30 min reaction time, is an indication of catalyst deactivation, when the hydrogenation of phenyl ring is retarded. The concentration of propylbenzene exhibited a maximum level at 90 min decreasing thereafter showing also that some activity was maintained.
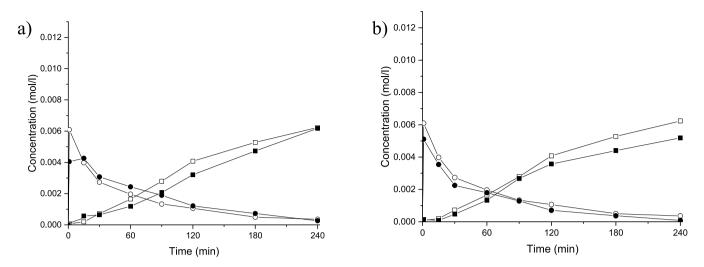
Figure 14. Molar concentration of dihydroeugenol (ball) and propylcyclohexane (squares) as a function of time over 11 wt % Co/SiO$_2$ in HDO of isoeugenol. Symbols: (a) The open symbol denotes catalyst reduced at 415 °C, and the solid symbol, that reduced at 550 °C. (b) The open symbols denote fresh catalyst and solid symbols regenerated and reused catalysts. Conditions: 300 °C and 30 bar hydrogen, initial isoeugenol concentration 0.012 mol/L.

The effect of the reduction temperature of 11 wt % Co/SiO$_2$ was also investigated in isoeugenol HDO (Figure 14a) at 300 °C and 30 bar showing similar catalytic behavior independent of the reduction temperature. In addition to cyclic products, also large amounts of hexane and heptane (20−38%) were formed. Despite similar GCLPA levels and product distributions in the liquid phase (Table 5), almost 2-fold more gaseous products (Figure 12) were formed over 11 wt % Co/SiO$_2$ reduced at 415 °C compared to reduction at a higher temperature (Figure 14a). High amounts of methane were formed in both cases, indicating cobalt ability to form methane in HDO of isoeugenol at 300 °C. Methane can be formed from methanol via dehydroxylation and hydrogenation. Since formation of methanol was not quantified in this work, it is difficult to draw detailed conclusions about the origin of methane formation.

Recyclability tests of 11 wt % Co/SiO$_2$ reduced at 415 °C were performed in HDO of isoeugenol at 300 °C and 30 bar (Figure 14b). The results showed that the performances of the fresh, spent, regenerated, and reduced catalysts are very similar.

CONCLUSIONS

Catalytic hydrodeoxygenation of the lignin-derived phenolic compound isoeugenol was investigated over cobalt- and nickel-based catalysts in a batch reactor at 200 and 300 °C and 30 bar total hydrogen pressure.

HDO of isoeugenol over cobalt-based catalysts showed that 300 °C is required for formation of propylcyclohexane. The yields of propylcyclohexane increased in the following order: Co/TiO$_2$ < Co/Al$_2$O$_3$ < Ni/SiO$_2$ < Co/SiO$_2$ < Ni/graphite < Co/SBA-15. HDO of isoeugenol over 20 wt % Ni/graphite and 11 wt % Ni/SiO$_2$ showed about the same concentrations of the intermediate compound propylcyclohexanone; however, its further transformation to propylcyclohexane over Ni/SiO$_2$ occurs slower than over Ni/graphite in line with its lower dispersion and lower hydrogenation ability. The yield of propylcyclohexane after 4 h was 60% over Ni/graphite and 44% over Ni/SiO$_2$ with GCLPA 73 and 70%, correspondingly, whereas Ni/graphite produced a more than 2-fold amount of

gaseous products (mainly methane) in comparison with Ni/SiO$_2$.

The highest yield of propylcyclohexane, 63%, and the highest sum of reactants and products in the liquid phase (GCLPA), 79%, were obtained over 10 wt % Co/SBA-15. A low sum of the concentrations of reactant and products in the liquid phase and a low propylcyclohexane yield, 10%, were observed for 15 wt % Co/Al$_2$O$_3$, which produced a high amount of methane. This catalyst with an acidic support promoted also formation of oligomers confirmed by size exclusion chromatography.

HDO of isoeugenol over an industrially relevant, 11 wt % Co/SiO$_2$ catalyst revealed that the reduction temperature does not affect the GCLPA giving the same GCLPA of 73%. This catalyst was also successfully regenerated and reused in isoeugenol hydrodeoxygenation giving 60% yield of propylcyclohexane.

ASSOCIATED CONTENT

Ⓢ Supporting Information

The Supporting Information is available free of charge on the ACS Publications website at DOI: 10.1021/acssuschemeng.9b02108.

> Catalyst reduction program; size exclusion chromatography results, ICP-MS data; TEM images of Co/TiO$_2$ and Co/Al$_2$O$_3$; diffractograms of 10 wt % Co/SBA-15, 15 wt % Co/Al$_2$O$_3$, 15 wt % CoTiO$_2$; TGA results of different catalysts (PDF)

AUTHOR INFORMATION

Corresponding Author

*Email: dmurzin@abo.fi.

ORCID Ⓘ

David Kubička: 0000-0003-2996-7824

Irina L. Simakova: 0000-0002-5138-4847

Dmitry Yu. Murzin: 0000-0003-0788-2643

Notes

The authors declare no competing financial interest.

■ REFERENCES

(1) Perlack, R. D.; Wright, L. L.; Turhollow, A. F.; Graham, R. L.; Stokes, B. J.; Erbach, D. C. *Biomass as Feedstock for a bioenergy and bioproducts industry: the technical feasibility of a billion-ton annual supply*; U.S Department of Energy, Oak Ridge 2005.

(2) Mäki-Arvela, P.; Murzin, D. Y. Hydrodeoxygenation of lignin-derived phenols: from fundamental studies towards industrial applications. *Catalysts* **2017**, *7* (9), 265.

(3) Zakzeski, J.; Bruijnincx, P.; Jongerius, A.; Weckhuysen, B. The catalytic valorization of lignin for the production of renewable chemicals. *Chem. Rev. (Washington, DC, U. S.)* **2010**, *110* (6), 3552–3599.

(4) European Parliament and the Council. *Directive 2009/28/EC*; 2009.

(5) Gupta, R. B.; Demirbas, A. *Gasoline, Diesel and Ethanol Biofuels from Grasses and Plants*; Cambridge University Press: New York, 2010.

(6) Schobert, H. *Chemistry of Fossil Fuels and Biofuels*; Cambridge University Press: New York, 2013.

(7) Ladisch, M.; Ximenes, E.; Kim, Y.; Mosier, N. S. Biomass chemistry. In *Catalysis for the Conversion of Biomass and Derivatives*; Behrens, M., Datye, A., Eds.; 2013; ISBN: 978-3-945561-19-5.

(8) Cherubini, F. The biorefinery concept: using biomass instead of oil for producing energy and chemicals. *Energy Convers. Manage.* **2010**, *51*, 1412–1421.

(9) Mendes, F. L.; da Silva, V. T.; Pacheco, M. E.; Toniolo, F. S.; Henriques, C. A. Bio-oil hydrotreating using nickel phosphides supported on carbon-covered alumina. *Fuel* **2019**, *241*, 686–694.

(10) Gonzalez, C.; Marin, P.; Diez, F. V.; Ordonez, S. Gas phase hydrodeoxygenation of benzaldehyde, benzyl alcohol, phenylacetate and anisole over precious metal catalysts. *Ind. Eng. Chem. Res.* **2016**, *55*, 2319–2327.

(11) Ghampson, I. T.; Sepulveda, C.; Garcia, R.; Fierro, J. L. G.; Escalona, N. Carbon nanofiber-supported ReOx catalysts for the hydrodeoxygenation of lignin-derived compounds. *Catal. Sci. Technol.* **2016**, *6*, 4356–4369.

(12) Zhang, X.; Tang, W.; Zhang, Q.; Wang, T.; Ma, L. Hydrodeoxygenation of lignin-derived phenolic compounds to hydrocarbon fuel over supported Ni-based catalysts. *Appl. Energy* **2018**, *227*, 73–79.

(13) Bomont, L.; Alda-Onggar, M.; Fedorov, V.; Aho, A.; Peltonen, J.; Eränen, K.; Peurla, M.; Kumar, N.; Wärnå, J.; Russo, V.; Mäki-Arvela, P.; Grenman, H.; Lindblad, M.; Murzin, D.Yu. Production of cycloalkanes in hydrodeoxygenation of isoeugenol over Pt- and Ir-modified bifunctional catalysts. *Eur. J. Inorg. Chem.* **2018**, *24*, 2841–2854.

(14) Alda-Onggar, M.; Maki-Arvela, P.; Eranen, K.; Aho, A.; Hemming, J.; Paturi, P.; Peurla, M.; Lindblad, M.; Simakova, I. L.; Murzin, D. Y. Hydrodeoxygenation of isoeugenol over alumina-supported Ir, Pt and Re catalysts. *ACS Sustain. Chem. Eng.* **2018**, *6*, 16205–16218.

(15) Bjelić, A.; Grilc, M.; Likozar, B. Catalytic hydrogenation and hydrodeoxygenation of lignin derived model compound eugenol over Ru/C: Intrinsic microkinetics and transport phenomena. *Chem. Eng. J.* **2018**, *333*, 240–259.

(16) Bjelic, A.; Grilc, M.; Hus, M.; Likozar, B. Hydrogenation and hydrodeoxygenation of aromatic lignin monomers over Cu/C, Ni/C, Pd/C, Pt/C, Rh/C and Ru/C catalysts: Mechanism, reaction microkinetic modelling and quantitative structure-activity relationship. *Chem. Eng. J.* **2019**, *359*, 305–320.

(17) Alda-Onggar, M.; Mäki-Arvela, P.; Aho, A.; Simakova, I.; Murzin, D. Yu. Hydrodeoxygenation of phenolic model compounds over zirconia supported Ir and Ni-catalysts. *React. Kinet., Mech. Catal.* **2019**, *126*, 737–759.

(18) Tieuli, S.; Mäki-Arvela, P.; Peurla, M.; Eränen, K.; Wärnå, J.; Cruciani, G.; Menegazzo, F.; Murzin, D. Yu.; Signoretto, M. Hydrodeoxygenation of isoeugenol over Ni-SBA-15: Kinetics and modelling. *Appl. Catal., A* **2019**, *580*, 1–10.

(19) Broglia, F.; Rimoldi, L.; Meroni, D.; De Vecchi, S.; Morbidelli, M.; Ardizzone, S. Guaiacol hydrodeoxygenation as a model lignin upgrading. Role of the support surface features on Ni-based alumina-silica catalysts. *Fuel* **2019**, *243*, 501–508.

(20) Roberts, E. J.; Habas, S. E.; Wang, L.; Ruddy, D. A.; White, E. A.; Baddour, F. G.; Griffin, M. B.; Schaidle, J. A.; Malmstadt, N.; Brutchey, R. L. High throughput continuous flow synthesis of nickel nanoparticles for the catalytic hydrodeoxygenation of guaiacol. *ACS Sustainable Chem. Eng.* **2017**, *5*, 632–639.

(21) Zhang, X.; Zhang, Q.; Wang, T.; Ma, L.; Yu, Y.; Chen, L. Hydrodeoxygenation of lignin-derived phenolic compounds to hydrocarbons over Ni/SiO$_2$–ZrO$_2$ catalysts. *Bioresour. Technol.* **2013**, *134*, 73–80.

(22) Liu, X.; Jia, W.; Xu, G.; Zhang, Y.; Fu, Y. Selective hydrodeoxygenation of lignin-derived phenols to cyclohexanols over Co-based catalysts. *ACS Sustainable Chem. Eng.* **2017**, *5*, 8594–8601.

(23) Brunauer, S.; Emmett, P. H.; Teller, E. Adsorption of gases in multimolecular layers. *J. Am. Chem. Soc.* **1938**, *60* (2), 309–319.

(24) Zaki, M. I.; Hasan, M. A.; Al-Sagheer, F.; Pasupulety, L. In situ FTIR spectra of pyridine adsorbed on SiO$_2$-Al$_2$O$_3$, TiO$_2$, ZrO$_2$ and CeO$_2$: general considerations for the identification of acid sites on surfaces of finely divided metal oxides. *Colloids Surf., A* **2001**, *190* (3), 261–274.

(25) Emeis, C. A. Determination of Integrated molar extinction coefficients for infrared absorption bands of pyridine adsorbed on solid acid catalysts. *J. Catal.* **1993**, *141*, 347–354.

(26) Lutterotti, L.; Bortolotti, M.; Ischia, G.; Lonardelli, I.; Wenk, H.-R. Rietveld texture analysis from diffraction images. *Z. Kristallogr. Suppl.* **2007**, *26*, 125–130.

(27) Abdullah, H. A.; Hauser, A.; Ali, F. A.; Al-Adwani, A. Optimal conditions for coke extraction of spent catalyst by accelerated solvent extraction compared to Soxhlet. *Energy Fuels* **2006**, *20* (1), 320–323.

(28) Martinez, A.; López, C.; Márquez, F.; Diaz, I. Fischer–Tropsch synthesis of hydrocarbons over mesoporous Co/SBA-15 catalysts: the influence of metal loading, cobalt precursor and promoters. *J. Catal.* **2003**, *220* (2), 486–499.

(29) Ning, W.; Shen, H.; Jin, Y.; Yang, X. Effects on weak surface modification on Co/SiO$_2$ Catalyst for Fischer–Tropsch reaction. *PLoS One* **2015**, *10* (5), No. e0124228.

(30) Xu, X.; Li, J.; Hao, Z.; Zhao, W.; Hu, C. Characterization and catalytic performance of Co/SBA-15 supported gold catalysts for CO oxidation. *Mater. Res. Bull.* **2006**, *41* (2), 406–413.

(31) Li, H.; Li, H.; Deng, J.-F. Influence on the reduction degree of Ni-B/SiO$_2$ amorphous catalyst and its role in selective hydrogenation of acrylonitrile. *Appl. Catal., A* **2000**, *193* (1–2), 9–15.

(32) Owen, E. A.; Jones, D. M. Effect of grain size on the crystal structure of cobalt. *Proceedings of the Physical Society, London* **1954**, *67*, 456–466.

(33) Theivasanthi, T.; Alagar, M. Titanium dioxide (TiO$_2$) nanoparticles XRD analyses: An insight. *Arxiv.org* **2013**, 1307.1091.

(34) Riva, R.; Miessner, H.; Vitali, R.; Del Piero, G. Metal-support interaction in Co/SiO$_2$ and Co/TiO$_2$. *Appl. Catal., A* **2000**, *196* (1), 111–123.

(35) Hu, L.; Yang, X.; Dang, S. An easily recyclable Co/SBA-15 catalyst: Heterogeneous activation of peroxymonosulfate for the degradation in water. *Appl. Catal., B* **2011**, *102* (1–2), 19–26.

(36) Lucredio, A. F.; Bellido, J. D. A.; Zawadzki, A.; Assaf, E. M. Co catalysts supported on SiO$_2$ and γ-Al$_2$O$_3$ applied to ethanol steam reforming: Effect of solvent used in the catalyst preparation method. *Fuel* **2011**, *90* (4), 1424–1430.

(37) Jacobs, G.; Chaney, J. A.; Patterson, P. M.; Das, T. K.; Davis, B. H. Fischer−Tropsch synthesis: study of the promotion of Re on the reduction property of Co/Al$_2$O$_3$ catalysts by in situ EXAFS/XANES of Co K and Re L$_{III}$ edges and XPS. *Appl. Catal., A* **2004**, *264* (2), 203−212.

(38) Gheitanchi, R.; Khodadadi, A. A.; Taghizadeh, M.; Mortazavi, Y. Effects of ceria addition and pre-calcination temperature on performance of cobalt catalysts for Fischer−Tropsch synthesis. *React. Kinet. Catal. Lett.* **2006**, *88* (2), 225−232.

(39) Khangale, P. R.; Meijboom, R.; Jalama, K. Reduction behaviour for Co/Al$_2$O$_3$ Fischer−Tropsch catalysts in presence of H$_2$ or CO. *Proceedings of the World Congress on Engineering*; 2014; p 2, http://www.iaeng.org/publication/WCE2014/WCE2014_pp1048-1051.pdf (accessed 6/15/2019).

(40) Xiong, H.; Zhang, Y.; Liew, K.; Li, J. Fischer−Tropsch synthesis: The role of pore size for Co/SBA-15 catalysts. *J. Mol. Catal. A: Chem.* **2008**, *295* (1−2), 68−76.

(41) Ghampson, I. T.; Sepulveda, C.; Garcia, R.; Radovic, L. R.; Fierro, J.L. G.; DeSisto, W. J.; Escalona, N. Hydrodeoxygenation of guaiacol over carbon-supported molybdenum nitride catalysts: Effects of nitriding and support properties. *Appl. Catal. A: Gen.* **2012**, *439−440*, 111−124.

(42) Zhang, H.; Shao, S.; Xiao, R.; Shen, D.; Zeng, J. Characterization of coke deposition in the catalytic fast pyrolysis of biomass derivatives. *Energy Fuels* **2014**, *28* (1), 52−57.

(43) Li, Y.; Zhang, C.; Liu, Y.; Hou, X.; Zhang, R.; Tang, X. Coke Deposition on Ni/HZSM-5 in bio-oil hydrodeoxygenation processing. *Energy Fuels* **2015**, *29* (3), 1722−1728.

(44) Zhan, J.; Wang, H.; Zhu, F.; Song, S. Analysis on the governing reactions in coal oxidation at temperatures up to 400 °C. *Int. J. Clean Coal Energy* **2014**, *3* (2), 19.

(45) Muley, P. D.; Henkel, C. E.; Aguilar, G.; Klasson, K. T.; Boldor, D. Ex situ thermo-catalytic upgrading of biomass pyrolysis vapors using a traveling wave microwave reactor. *Appl. Energy* **2016**, *183*, 995−1004.

(46) Jang, M. S.; Phan, T. N.; Chung, I. S.; Lee, I.-G.; Park, Y.-K.; Ko, C. H. Metallic nickel supported on mesoporous silica as catalyst for hydrodeoxygenation: effect on pore size and structure. *Res. Chem. Intermed.* **2018**, *44* (6), 3723−3735.

(47) Tran, T. T. N.; Uemura, Y.; Chowdhury, S.; Ramli, A. Vapor-phase hydrodeoxygenation of guaiacol on Al-MCM-41 supported Ni and Co catalysts. *Appl. Catal., A* **2016**, *512*, 93−100.